



# Calculation of global optimal initial and boundary perturbations for the linearised incompressible Navier–Stokes equations

Xuerui Mao <sup>a,\*</sup>, Hugh M. Blackburn <sup>a</sup>, Spencer J. Sherwin <sup>b</sup>

<sup>a</sup> Department of Mechanical and Aerospace Engineering, Monash University, Melbourne 3800, Australia

<sup>b</sup> Department of Aeronautics, Imperial College London, South Kensington, SW7 2AZ, UK

## ARTICLE INFO

### Article history:

Received 8 February 2012

Received in revised form 19 October 2012

Accepted 28 October 2012

Available online 23 November 2012

### Keywords:

Optimal perturbation

Adjoint equation

Optimisation

## ABSTRACT

This study considers numerical methods for computation of optimal boundary and initial perturbations to incompressible flows. Similar to previous work, constrained Lagrangian functionals are built and gradient optimisation methods are applied to optimise perturbations that maximise the energy of perturbations in the computational domain at a given time horizon. Unlike most of the previous work in this field we consider both optimal initial and boundary condition problems and demonstrate how each can be transformed into an eigenvalue problem. It is demonstrated analytically and numerically that both optimisation and eigenvalue approaches converge to the same outcome, even though the optimisation approach may converge more slowly owing to the large number of inflection points. In a case study, these tools are used to calculate optimal initial and boundary perturbations to the Batchelor vortex. It is observed that when the flow is asymptotically stable, the optimal inflow perturbation is similar to the most unstable local eigenmode, while when the flow is stable/weakly unstable, the spatial distribution of the optimal inflow perturbation is similar to the local optimal initial perturbation.

© 2012 Elsevier Inc. All rights reserved.

## 1. Introduction

It is well-known that the evolution operators of perturbations in many open/closed flows are highly non-normal. The non-orthogonality of the eigenmodes of these operators can induce significant transient energy growth over short time intervals [1,2]. When the flow is asymptotically stable or weakly unstable, transient response to perturbations may induce significant change to the flow over finite time horizons.

Perturbations that maximise the energy in the response perturbation flow field are referred to as optimal. The optimal perturbation in the form of initial conditions has been extensively investigated in both local and global frameworks [2–4]. In steady or periodic base flows, the optimal initial perturbation is a linear combination of the eigenmodes of the evolution operator and over large time intervals, it approaches the leading adjoint eigenmode [5].

In local studies where the discretised matrix of the evolution operator is explicitly available, the optimal perturbation can be calculated through a singular value decomposition of the fully discretised operator, where the square of the largest singular value is the optimal energy growth and the corresponding right and left singular vectors are the optimal perturbation and its response, respectively [3].

Under more general conditions where the matrix form of the discretised operator is not available, commonly in global studies with large-dimensional base flows which are inhomogeneous in at least two directions, the optimal initial

\* Corresponding author. Present address: School of Engineering and Computing Sciences, Durham University, DH1 3LE, UK.

E-mail address: [xuerui.mao@durham.ac.uk](mailto:xuerui.mao@durham.ac.uk) (X. Mao).

perturbation can be calculated through an iterative method, such as an eigenvalue method or an optimisation method. In the eigenvalue method, the optimal perturbation and energy growth are considered as the leading eigenvector/value of a joint operator, whose action is to integrate the perturbation forwards through the linearised evolution operator and then backwards through the adjoint operator [4,6–8]. Instead of discretizing this joint operator and building the matrix form of it directly, a Krylov sequence consisting of the iterative outcomes of this operator is constructed, and then an Arnoldi method or the Lanczos method is adopted to extract the leading eigenvector/eigenvalue of this joint operator. In this approach, the objective can be changed by merely changing the inner product weight in the definition of norms of the initial and final perturbations. [9] have used this eigenvalue approach to calculate the optimal upstream disturbance that experiences largest energy growth at a fixed downstream location in boundary layer flow. In the optimisation method, a constrained Lagrangian functional is built and the optimal perturbation is the velocity vector which maximises the Lagrangian functional [2,10,11]. This optimisation method has also been adopted to calculate the nonlinear optimal initial perturbations by [12,13]. In the latter work, the time-averaged dissipation, instead of the kinetic energy at a final time that is used commonly in the literature when defining an optimal perturbation, is chosen as the objective functional for better numerical convergence. These two approaches are discussed by [14] when solving optimal initial perturbations and optimal forcing localised in space in the Blasius boundary-layer flow and good agreement between the approaches is presented.

The complementary branch of the optimal perturbation problem –the optimal boundary perturbation problem – has received relatively limited attention. In local studies, some algorithms to calculate the boundary control velocity vectors have been proposed [10,11], but these algorithms are restrained to the context of parallel base flows and cannot be extended to global studies without significant modifications. Most recently [15] have proposed an optimisation algorithm to calculate the optimal spatial distribution of the inflow boundary perturbation to a stenotic flow, where the outflow velocity boundary condition is set to zero Dirichlet conditions, providing that the domain is adequately long.

In this work, we first outline the optimisation and eigenvalue methods for global initial perturbations, and then, develop an eigenvalue solver to compute the optimal boundary perturbations and demonstrate that this eigenvalue algorithm is equivalent to the reported optimisation approach [15]. A Robin outflow boundary condition is adopted to release the restriction on the size of the domain. Finally we implement these new numerical tools to calculate the optimal inflow boundary perturbation to a vortex flow as a case study.

## 2. Problem definition

Working from the incompressible Navier–Stokes equations

$$\partial_t \mathbf{u} = -\mathbf{u} \cdot \nabla \mathbf{u} - \nabla p + Re^{-1} \nabla^2 \mathbf{u}, \quad \text{with } \nabla \cdot \mathbf{u} = 0,$$

where  $p$  is the modified or kinematic pressure, and  $\mathbf{u}$  is the velocity vector, decomposing the flow field as the sum of a base flow and a perturbation i.e.  $(\mathbf{u}, p) = (\mathbf{U}, P) + (\mathbf{u}', p')$  and omitting the interaction of perturbations, we obtain the linearised Navier–Stokes (LNS) equations, which govern the evolution of perturbations, as

$$\partial_t \mathbf{u}' = -\mathbf{U} \cdot \nabla \mathbf{u}' - (\nabla \mathbf{U})^T \cdot \mathbf{u}' - \nabla p' + Re^{-1} \nabla^2 \mathbf{u}', \quad \text{with } \nabla \cdot \mathbf{u}' = 0,$$

or more compactly, considering pressure is a dependent variable,

$$\partial_t \mathbf{u}' - L(\mathbf{u}') = 0. \tag{1}$$

If the base flow is homogeneous in the azimuthal direction in the cylindrical coordinates  $(z, r, \theta)$ , we can further decompose the perturbation field into azimuthal Fourier modes, each of which will evolve independently, such that:

$$(\mathbf{u}', p') = (u', v', w', p') = [u'_m(r, z), v'_m(r, z), w'_m(r, z), p'_m(r, z)] \exp(im\theta),$$

where  $m$  denotes an integer azimuthal wavenumber. If the base flow is homogeneous in the spanwise direction in a Cartesian coordinate, a similar spanwise Fourier mode can be defined at a real spanwise wavenumber. To keep notation reasonably compact in what follows we implicitly adopt Fourier decomposition for the perturbation field, only introduce its azimuthal/spanwise Fourier mode index  $m$  when required, and suppress representation of  $\theta$ -dependence. In a similar vein, since we mainly consider perturbation fields in the following, the prime ( $\prime$ ) notation for perturbation variables is omitted hereafter.

We introduce scalar products defined on spatial domain  $\Omega$  and its boundary  $\partial\Omega$

$$\begin{aligned} \langle \mathbf{a}, \mathbf{b} \rangle &= \int_{\Omega} \mathbf{a} \cdot \mathbf{b} dV, & \langle \mathbf{a}, \mathbf{b} \rangle &= \int_0^{\tau} \int_{\Omega} \mathbf{a} \cdot \mathbf{b} dV dt, \\ \{ \mathbf{c}, \mathbf{d} \} &= D \int_{\partial\Omega} \mathbf{c} \cdot \mathbf{d} dS, & \{ \mathbf{c}, \mathbf{d} \} &= D \int_0^{\tau} \int_{\partial\Omega} \mathbf{c} \cdot \mathbf{d} dS dt, \end{aligned}$$

where  $\mathbf{a}, \mathbf{b} \in [0, \tau] \times \Omega$  and  $\mathbf{c}, \mathbf{d} \in [0, \tau] \times \partial\Omega$ .  $D$  is a spatial length scale introduced into these definitions in order to maintain dimensional homogeneity as discussed below.

The optimal initial condition problem can be expressed as seeking an initial perturbation to maximise the energy growth over time interval  $\tau$ , defined as the ratio of final energy at time  $\tau$  and the initial energy at time 0 and denoted as  $G$ ; the

optimal boundary condition problem can be expressed as seeking the boundary perturbations to maximise the gain, defined as the ratio of final energy at time  $\tau$  and a measurement of the boundary perturbation, denoted as  $K$ . Hence

$$G = \max_{\mathbf{u}_0} \frac{(\mathbf{u}_\tau, \mathbf{u}_\tau)}{(\mathbf{u}_0, \mathbf{u}_0)} \quad \text{and} \quad K = \max_{\mathbf{u}_c} \frac{(\mathbf{u}_\tau, \mathbf{u}_\tau)}{\{\mathbf{u}_c, \mathbf{u}_c\}},$$

where  $\mathbf{u}_0 \in \Omega$  denotes the initial perturbation velocity vector,  $\mathbf{u}_c \in \partial\Omega$  represents the boundary velocity vector and  $\mathbf{u}_\tau \in \Omega$  is the response velocity vector at time  $\tau$ . In the initial value problem we set the boundary perturbation to zero, while in the boundary value problem we set the initial perturbation to zero in order to isolate the developments of initial and boundary perturbations and make the ratios  $G$  and  $K$  independent of the magnitude of initial or boundary perturbations.

To reduce the dimension of  $\mathbf{u}_c$ , we separate the spatial and temporal dependencies and specify the temporal dependence explicitly, such that e.g.

$$\mathbf{u}_c(r, z, t) = \hat{\mathbf{u}}_c(r, z)f(t, \omega),$$

The function  $f(t, \omega)$  contains terms to eliminate temporal and spatial discontinuity when integrating the governing equations, and when the final time  $\tau$  is large enough, this decomposition tends to the Fourier decomposition with  $\omega$  acting as the frequency, as addressed in detail in Section 4.1. Therefore in the optimal boundary problem, we only optimise the spatial dependence function  $\hat{\mathbf{u}}_c(r, z)$ . Correspondingly the object to maximise becomes

$$K = \max_{\hat{\mathbf{u}}_c} \frac{(\mathbf{u}_\tau, \mathbf{u}_\tau)}{[\hat{\mathbf{u}}_c, \hat{\mathbf{u}}_c]}$$

where we observe that  $f(t, \omega)$  is spatially constant and has the effect of uniformly scaling  $\mathbf{u}_\tau$  and so is not included. Note that  $K$  is dimensionless regardless of the system of spatial measurement adopted, but is particular to the choice of  $f(t, \omega)$ .

### 3. Optimal initial perturbations

In this section, we review the methodology to optimise the initial perturbations (Section 3.1) and demonstrate that this optimisation problem can be transformed into an eigenvalue problem (Section 3.2).

#### 3.1. Optimisation approach

Schmid [2] discussed a Lagrangian approach to computing the optimal initial perturbation. The Lagrangian functional to be optimised or maximised can be written as

$$\mathcal{L}_o = \frac{(\mathbf{u}_\tau, \mathbf{u}_\tau)}{(\mathbf{u}_0, \mathbf{u}_0)} - \left\langle \mathbf{u}^*, \frac{\partial \mathbf{u}}{\partial t} - L(\mathbf{u}) \right\rangle, \tag{2}$$

where the first term is the energy ratio  $G$  to be maximised and the second term is a dynamic constraint enforcing the LNS equations. Note that this definition is equivalent to that defined by [2,10], which contains three terms (the extra term is a constraint that the initial condition of the optimisation loop is equal to the optimal initial perturbation) and all the equations derived from these two forms of Lagrangian functional are the same. We note that the objective function, which is the energy growth in (2), can be simplified as the final kinetic energy by adding an explicit constraint that the initial perturbation has unit norm [14].

In order to simplify taking variations with respect to the perturbation field  $\mathbf{u}$ , we integrate the second term in Eq. (2) by parts [4] to obtain

$$\begin{aligned} -\langle \mathbf{u}^*, \partial_t \mathbf{u} - L(\mathbf{u}) \rangle &= \langle \mathbf{u}, \partial_t \mathbf{u}^* + L^*(\mathbf{u}^*) \rangle + \int_0^\tau \int_\Omega -\partial_t(\mathbf{u} \cdot \mathbf{u}^*) dV dt + \int_0^\tau \int_\Omega \nabla \cdot [-\mathbf{U}(\mathbf{u} \cdot \mathbf{u}^*) + \mathbf{u}p^* - \mathbf{u}^*p \\ &\quad + Re^{-1}(\nabla \mathbf{u} \cdot \mathbf{u}^* - \nabla \mathbf{u}^* \cdot \mathbf{u})] dV dt, \end{aligned} \tag{3}$$

where  $L^*(\mathbf{u}^*) = \mathbf{U} \cdot \nabla \mathbf{u}^* - \nabla \mathbf{U} \cdot \mathbf{u}^* - \nabla p^* + Re^{-1} \nabla^2 \mathbf{u}^*$  with  $\nabla \cdot \mathbf{u}^* = 0$ . The partial differential equation

$$\partial_t \mathbf{u}^* + L^*(\mathbf{u}^*) = 0 \tag{4}$$

is referred to as the adjoint of the LNS equations in the literature [16]. We note that this equation should be integrated backwards from  $t = \tau$  to  $t = 0$ , since otherwise it contains a negative diffusion operator. Using the divergence theorem, the last integral in (3) can be stated using only boundary terms so that

$$\begin{aligned} -\langle \mathbf{u}^*, \partial_t \mathbf{u} - L(\mathbf{u}) \rangle &= \langle \mathbf{u}, \partial_t \mathbf{u}^* + L^*(\mathbf{u}^*) \rangle + \int_0^\tau \int_\Omega -\partial_t(\mathbf{u} \cdot \mathbf{u}^*) dV dt + \int_0^\tau \int_{\partial\Omega} \mathbf{n} \cdot [-\mathbf{U}(\mathbf{u} \cdot \mathbf{u}^*) + \mathbf{u}p^* - \mathbf{u}^*p \\ &\quad + Re^{-1}(\nabla \mathbf{u} \cdot \mathbf{u}^* - \nabla \mathbf{u}^* \cdot \mathbf{u})] dS dt, \end{aligned} \tag{5}$$

where  $\mathbf{n}$  is a unit outward normal vector on the boundary of the domain,  $\partial\Omega$ .

As stated above, when calculating the optimal initial perturbation, the contributions of boundary perturbations are set to zero. Adopting zero-Dirichlet boundary conditions for the velocity components for both LNS equations and the adjoint equations, the last term on the right hand side of (5) becomes zero, and therefore

$$\mathcal{L}_0 = \frac{(\mathbf{u}_\tau, \mathbf{u}_\tau)}{(\mathbf{u}_0, \mathbf{u}_0)} + \left\langle \mathbf{u}, \frac{\partial \mathbf{u}^*}{\partial t} + L^*(\mathbf{u}^*) \right\rangle - (\mathbf{u}_\tau^*, \mathbf{u}_\tau) + (\mathbf{u}_0^*, \mathbf{u}_0). \tag{6}$$

Setting to zero the first variations of  $\mathcal{L}_0$  with respect to its independent variables  $\mathbf{u}^*$ ,  $\mathbf{u}$  and  $\mathbf{u}_\tau$  yields the following set of equations:

$$\delta \mathcal{L}_0(\delta \mathbf{u}^*) = 0 \Rightarrow \frac{\partial \mathbf{u}}{\partial t} - L(\mathbf{u}) = 0, \tag{7}$$

$$\delta \mathcal{L}_0(\delta \mathbf{u}) = 0 \Rightarrow \frac{\partial \mathbf{u}^*}{\partial t} + L^*(\mathbf{u}^*) = 0, \tag{8}$$

$$\delta \mathcal{L}_0(\delta \mathbf{u}_\tau) = 0 \Rightarrow \mathbf{u}_\tau^* = \frac{2\mathbf{u}_\tau}{(\mathbf{u}_0, \mathbf{u}_0)}. \tag{9}$$

The first two equations recover the LNS equations and the adjoint equations, while the third initialises the adjoint equations at  $t = \tau$  with the scaled final condition of the LNS equations since the adjoint equations are integrated backwards.

The variations of the Lagrangian functional with respect to the initial condition  $\mathbf{u}_0$  can be written as

$$\delta \mathcal{L}_0(\delta \mathbf{u}_0) = \left( \mathbf{u}_0^* - \frac{2(\mathbf{u}_\tau, \mathbf{u}_\tau)}{(\mathbf{u}_0, \mathbf{u}_0)^2} \mathbf{u}_0, \delta \mathbf{u}_0 \right). \tag{10}$$

Using the definition of the gradient of the Lagrangian associated with the Gâteaux differential given by [10], the gradient of the Lagrangian functional with respect to the initial condition  $\mathbf{u}_0$  can be expressed as

$$\nabla_{\mathbf{u}_0} \mathcal{L}_0 = \mathbf{u}_0^* - \frac{2(\mathbf{u}_\tau, \mathbf{u}_\tau)}{(\mathbf{u}_0, \mathbf{u}_0)^2} \mathbf{u}_0. \tag{11}$$

A gradient method is used to optimise  $\mathbf{u}_0$  to reach maxima of  $G$  and an optimal step length is obtained by exploiting the linear feature of the governing equations to update  $\mathbf{u}_0$  during the optimisation process. The optimisation procedure is detailed in A.

### 3.2. Eigenvalue approach

As an alternative to the optimisation approach described above, [4] outlined an eigenvalue method based on primitive variables to calculate the global optimal initial conditions. [14] have also used both approaches to calculate the optimal initial perturbations and optimal forcing and demonstrated good agreement. Below we demonstrate that the optimisation and eigenvalue approaches are equivalent. We define two transform operators to represent the actions of the LNS equations and the adjoint equations,

$$\mathbf{u}_\tau = \mathcal{M}_0 \mathbf{u}_0 \quad \text{and} \quad \mathbf{u}_0^* = \mathcal{M}_0^* \mathbf{u}_\tau^*. \tag{12}$$

Comparing the two forms of the Lagrangian functional in equations (2) and (6), we see that

$$(\mathbf{u}_\tau^*, \mathcal{M}_0 \mathbf{u}_0) = (\mathcal{M}_0^* \mathbf{u}_\tau^*, \mathbf{u}_0).$$

Therefore  $\mathcal{M}_0^*$  is the adjoint operator of  $\mathcal{M}_0$  with respect to the inner product  $(\cdot, \cdot)$ . Substituting  $\mathcal{M}_0$  and  $\mathcal{M}_0^*$  into the Lagrangian functional, we see that the Lagrangian can be expressed as a function of  $\mathbf{u}_0$ ,

$$\mathcal{L}_0 = \frac{(\mathbf{u}_0, \mathcal{M}_0^* \mathcal{M}_0 \mathbf{u}_0)}{(\mathbf{u}_0, \mathbf{u}_0)}. \tag{13}$$

Clearly the maximum value of the Lagrangian functional is the largest eigenvalue of the symmetric operator  $\mathcal{M}_0^* \mathcal{M}_0$ , and the corresponding eigenvector is the optimal initial perturbation. Next we demonstrate that the eigenvector corresponding to the largest eigenvalue of  $\mathcal{M}_0^* \mathcal{M}_0$  is the only maximiser of the Lagrangian functional even though this functional is not concave, and thus in the optimisation method the initial perturbation converges to the largest eigenvector of  $\mathcal{M}_0^* \mathcal{M}_0$ . Taking the variation of the Lagrangian functional (13) with respect to  $\mathbf{u}_0$  produces

$$\delta \mathcal{L}_0(\delta \mathbf{u}_0) = \frac{2(\delta \mathbf{u}_0, \mathcal{M}_0^* \mathcal{M}_0 \mathbf{u}_0)}{(\mathbf{u}_0, \mathbf{u}_0)} - \frac{2(\mathbf{u}_0, \mathcal{M}_0^* \mathcal{M}_0 \mathbf{u}_0)(\delta \mathbf{u}_0, \mathbf{u}_0)}{(\mathbf{u}_0, \mathbf{u}_0)^2}. \tag{14}$$

Substituting (9) and (12) into (14), it can be seen that this expression of first variation is equivalent to (10). In the discussions above, the operators are kept in continuous forms and therefore have infinite dimensions. After spatial discretization, all the vectors and operators have finite dimensions. Assuming that the optimal initial perturbation is discretised to an  $N$  dimensional vector, then the joint operator  $\mathcal{M}_0^* \mathcal{M}_0$  is discretised to an  $N \times N$  matrix. Since this operator is self-adjoint, the

corresponding matrix will have  $N$  real eigenvalues and  $N$  orthogonal eigenvectors. We denote the eigenvalue and eigenvector pairs of this matrix as  $\lambda_i$  and  $\mathbf{v}_i$  with  $i = 1, \dots, N$  and  $0 \leq \lambda_1 \leq \lambda_2 \leq \dots \leq \lambda_N$ . For convenience we consider that the eigenvectors are normalised so that  $(\mathbf{v}_i, \mathbf{v}_i) = 1$ . We note that as the spatial discretization is refined,  $N$  increases and the smallest eigenvalue  $\lambda_1$  tends to zero.

We see that the variation of the Lagrangian functional in (14) is zero, at and only at  $\mathbf{u}_0 = \mathbf{v}_i$ . We now calculate the second order variation to see if  $\mathbf{u}_0 = \mathbf{v}_i$  are local or global maximisers of the Lagrangian functional:

$$\delta^2 \mathcal{L}_0(\delta \mathbf{u}_0) = -\frac{2(\mathbf{u}_0, \mathcal{M}_0^* \mathcal{M}_0 \mathbf{u}_0)(\delta \mathbf{u}_0, \delta \mathbf{u}_0)}{(\mathbf{u}_0, \mathbf{u}_0)^2} - \frac{8(\delta \mathbf{u}_0, \mathcal{M}_0^* \mathcal{M}_0 \mathbf{u}_0)(\mathbf{u}_0, \delta \mathbf{u}_0)}{(\mathbf{u}_0, \mathbf{u}_0)^2} + \frac{2(\delta \mathbf{u}_0, \mathcal{M}_0^* \mathcal{M}_0 \delta \mathbf{u}_0)}{(\mathbf{u}_0, \mathbf{u}_0)} + \frac{8(\mathbf{u}_0, \mathcal{M}_0^* \mathcal{M}_0 \mathbf{u}_0)(\delta \mathbf{u}_0, \mathbf{u}_0)^2}{(\mathbf{u}_0, \mathbf{u}_0)^3}. \tag{15}$$

At the stationary points where  $\mathbf{u}_0 = \mathbf{v}_i$ , the second and fourth terms on the right side of Eq. (15) are balanced and the second order variation becomes

$$\delta^2 \mathcal{L}_0(\delta \mathbf{u}_0) = \frac{2}{(\mathbf{u}_0, \mathbf{u}_0)} ((\delta \mathbf{u}_0, \mathcal{M}_0^* \mathcal{M}_0 \delta \mathbf{u}_0) - (\delta \mathbf{u}_0, \delta \mathbf{u}_0) \lambda_i). \tag{16}$$

We see that the sign of the second order variation depends on the second factor on the right side of Eq. (16). Since the eigenvectors of  $\mathcal{M}_0^* \mathcal{M}_0$ ,  $\mathbf{v}_i$  are orthogonal,  $\delta \mathbf{u}_0$  can be represented as

$$\delta \mathbf{u}_0 = \sum_{j=1}^N a_j \mathbf{v}_j, \tag{17}$$

Recalling that  $(\mathbf{v}_j, \mathbf{v}_j) = 1$ , we have

$$(\delta \mathbf{u}_0, \mathcal{M}_0^* \mathcal{M}_0 \delta \mathbf{u}_0) = \sum_{j=1}^N a_j^2 \lambda_j, \quad \text{and} \quad (\delta \mathbf{u}_0, \delta \mathbf{u}_0) \lambda_i = \lambda_i \sum_{j=1}^N a_j^2, \tag{18}$$

Substituting (18) into (16), we see that if  $\lambda_i = \lambda_1$ ,  $\delta^2 \mathcal{L}_0 \geq 0$  ( $\delta^2 \mathcal{L}_0 = 0$  is satisfied when  $a_2, \dots, a_N = 0$ ); if  $\lambda_i = \lambda_N$ ,  $\delta^2 \mathcal{L}_0 \leq 0$  ( $\delta^2 \mathcal{L}_0 = 0$  is satisfied when  $a_1, \dots, a_{N-1} = 0$ ); if  $\lambda_i \neq \lambda_1$  and  $\lambda_i \neq \lambda_N$ , the sign of  $\delta^2 \mathcal{L}_0$  depends on the values of  $a_1, \dots, a_N$ . Therefore  $\mathbf{u}_0 = \mathbf{v}_1$  is the global minimiser of the Lagrangian functional and this minimum value is  $\lambda_1$ ;  $\mathbf{u}_0 = \mathbf{v}_N$  is the global maximiser and this maximum value is  $\lambda_N$ ;  $\mathbf{u}_0 = \mathbf{v}_2, \dots, \mathbf{v}_{N-1}$  provide inflection points rather than minima or maxima. These equilibrium states are schematically illustrated in Fig. 1. Theoretically the optimisation could terminate at either the maximum or inflection points. However, considering that the inflection points are sensitive to disturbances, the only robust solution for the optimisation is the global maximum  $\mathbf{u}_0 = \mathbf{v}_N$ . At this maximum, we note that  $\mathcal{L}_0 = G = \lambda_N$ . It is worth noticing that a refinement of the spatial discretization results in a larger  $N$  and subsequently more inflection points. Therefore if the eigenpair  $(\lambda_N, \mathbf{v}_N)$  is not dominant among all the pairs, a finer discretization is expected to result in a slower convergence.

The eigenvalues/eigenvectors of the operator  $\mathcal{M}_0^* \mathcal{M}_0$  can be calculated by building a Krylov sequence through iteratively integrating a random initial perturbation forwards in the LNS equations and backwards in the adjoint equations and then using an Arnoldi method to extract the leading eigenvalues/eigenvectors [4].

If the matrix form of the forward operator  $\mathcal{M}_0$  were available, one could alternatively obtain the optimal initial perturbation, optimal energy growth and optimal response from the singular value decomposition of  $\mathcal{M}_0$ :

$$\mathcal{M}_0 \mathbf{U}_{0i} = \sigma_{0i} \mathbf{V}_{0i}. \tag{19}$$

The right and left singular vectors  $\mathbf{U}_{0i}$  and  $\mathbf{V}_{0i}$  form two orthogonal bases, normalised so that  $(\mathbf{U}_{0i}, \mathbf{U}_{0i}) = 1$  and  $(\mathbf{V}_{0i}, \mathbf{V}_{0i}) = 1$ . The singular values  $\sigma_i$  are real and positive. Clearly the largest singular value is the square root of the optimal energy growth and the corresponding right and left singular vectors are the optimal initial perturbation and the optimal outcome. This singular value decomposition approach is a direct method and only the forward operator  $\mathcal{M}_0$  is involved. In general, the matrix

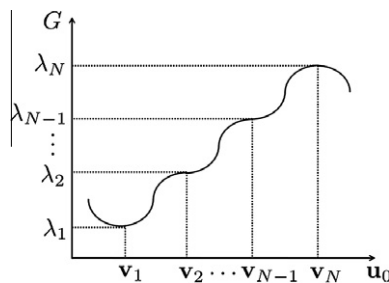


Fig. 1. Schematic representation of the maximum, minimum and inflection points of the energy growth  $G$  as a function of the initial perturbation  $\mathbf{u}_0$ . The eigenvectors in space  $\mathbb{R}^N$  are aligned along a one dimensional axis.

corresponding to the action of  $\mathcal{M}_0$  after spatial and temporal discretization is not available and iterative methods, e.g. eigenvalue methods or optimisation methods have to be adopted.

#### 4. Optimal boundary perturbations

In this section, we present a methodology to compute the other type of optimal perturbations considered in this work – optimal Dirichlet-type boundary perturbations that maximise the energy of the response perturbation field over a fixed time interval. In the following, we denote the segment of the boundary where the perturbation is introduced as the perturbation boundary. As in Section 3, we first introduce the optimisation algorithm (Section 4.1), and then transform it into an eigenvalue method (Section 4.2).

##### 4.1. Optimisation approach

Analogously to the analysis of the optimal initial condition problem, a Lagrangian functional for the optimal boundary perturbation can be expressed as

$$\mathcal{L}_c = \frac{(\mathbf{u}_\tau, \mathbf{u}_\tau)}{[\hat{\mathbf{u}}_c, \hat{\mathbf{u}}_c]} - \langle \mathbf{u}^*, \partial_t \mathbf{u} - L(\mathbf{u}) \rangle, \tag{20}$$

where the first term is the gain to be maximised and the second term is the constraint of the LNS equation.

Setting the adjoint velocity variables to zero on the boundary,  $\mathbf{u}^*(\partial\Omega) = 0$  and using zero initial conditions, we integrate the second term by parts to obtain

$$\mathcal{L}_c = \frac{(\mathbf{u}_\tau, \mathbf{u}_\tau)}{[\hat{\mathbf{u}}_c, \hat{\mathbf{u}}_c]} + \langle \mathbf{u}, \partial_t \mathbf{u}^* + L^*(\mathbf{u}^*) \rangle - (\mathbf{u}_\tau^*, \mathbf{u}_\tau) + \left[ \int_0^\tau (p^* \mathbf{n} - Re^{-1} \nabla_n \mathbf{u}^*) f^*(t, \omega) dt, \hat{\mathbf{u}}_c \right], \tag{21}$$

where  $f^*(t, \omega)$  is the adjoint of  $f(t, \omega)$ .

In previous studies of local optimal boundary perturbations [10,11,17], the integration in the last expression of (21) vanishes because the pressure and a velocity component are eliminated through algebraic manipulations of the localised governing equations and both zero-Dirichlet and zero-Neumann conditions were enforced on the adjoint velocity components on the perturbation boundary. In studies when the pressure term cannot be eliminated analytically, this integral has to be taken into account. In the methodology to calculate the global optimal inflow perturbation for a stenotic flow presented in [15], a zero pressure condition was imposed on the inflow boundary to simplify the calculation. In the current work, a computed Neumann pressure boundary condition is adopted so as to relax the zero pressure simplification; such boundary conditions are consistent with a velocity correction scheme [18]. Setting to zero the first variations of  $\mathcal{L}_c$  with respect to its independent variables  $\mathbf{u}^*$ ,  $\mathbf{u}$  and  $\mathbf{u}_\tau$  yields the following set of equations:

$$\delta \mathcal{L}_c(\delta \mathbf{u}^*) = 0 \Rightarrow \partial_t \mathbf{u} - L(\mathbf{u}) = 0, \tag{22}$$

$$\delta \mathcal{L}_c(\delta \mathbf{u}) = 0 \Rightarrow \partial_t \mathbf{u}^* + L^*(\mathbf{u}^*) = 0, \tag{23}$$

$$\delta \mathcal{L}_c(\delta \mathbf{u}_\tau) = 0 \Rightarrow \mathbf{u}_\tau^* = \frac{2\mathbf{u}_\tau}{[\hat{\mathbf{u}}_c, \hat{\mathbf{u}}_c]}. \tag{24}$$

In the above, (22) are the LNS equations as previously defined in Eq. (1), which evolve the velocity perturbation  $\mathbf{u}_c$  forwards in time from  $t = 0$  to  $t = \tau$  but now subject to inhomogeneous boundary conditions, (23) are the adjoint equations, which evolve the adjoint velocity  $\mathbf{u}_\tau^*$  backwards from  $t = \tau$  to  $t = 0$ , while (24) scales the outcome of the LNS equations at time  $t = \tau$  in order to initialise the adjoint equations. The gradient of the Lagrangian functional with respect to the spatial distribution of the boundary condition  $\hat{\mathbf{u}}_c$  can be expressed as

$$\nabla_{\hat{\mathbf{u}}_c} \mathcal{L}_c = \frac{-2(\mathbf{u}_\tau, \mathbf{u}_\tau)}{[\hat{\mathbf{u}}_c, \hat{\mathbf{u}}_c]^2} \hat{\mathbf{u}}_c + \mathbf{g}(\mathbf{u}^*, p^*, \omega), \tag{25}$$

where

$$\mathbf{g}(\mathbf{u}^*, p^*, \omega) = \int_0^\tau (p^* \mathbf{n} - Re^{-1} \nabla_n \mathbf{u}^*) f^*(t, \omega) dt.$$

We note that for the perturbation boundary, other valid combinations of boundary conditions exist for the adjoint velocity variables besides the zero Dirichlet condition, i.e.

$$\nabla_n \mathbf{u}^* + \frac{Rep - \nabla_n \mathbf{u}}{\mathbf{u}} \mathbf{u}^* = 0, \quad \text{with } p^* = 0, \tag{26}$$

where the factor  $(Rep - \nabla_n \mathbf{u})/\mathbf{u}$  (calculated component-by-component so that each term in this ratio is scalar) is calculated and stored in the forward integration of (22) and substituted into the Robin condition (26) at every time step during the backward integration of (23). For this boundary condition the definition of  $\mathbf{g}$  becomes

$$\mathbf{g}(\mathbf{u}^*, p^*, \omega) = \int_0^\tau (-\mathbf{n} \cdot \mathbf{U}) \mathbf{u}^* f^*(t, \omega) dt.$$

This ‘outflow’ type condition on the adjoint variable might be considered as more appropriate if the perturbation boundary is the inflow boundary and one follows the heuristic argument that the ‘inflow’ boundary for the LNS equations is an ‘outflow’ boundary condition for the adjoint equations owing to the change in sign of the advection terms. It has been demonstrated however that both sets of boundary conditions lead to the same value of gain [15]. This combination of boundary conditions also requires extra memory (to store  $(\text{Rep} - \nabla_n \mathbf{u})/\mathbf{u}$ ) and more computer time owing to the update of the Robin condition for velocities in the backward integration. Therefore in the present work we did not employ this combination but instead took  $\mathbf{u}^* = 0$  as noted above.

To summarise the initial and boundary conditions used in the optimal boundary condition problem, we adopt the following approach. The initial condition for the LNS equations is  $\mathbf{u}_0 = 0$  on the interior of the domain  $\Omega$ . For evolution of the adjoint equations, the initial adjoint state (at time  $\tau$ ),  $\mathbf{u}_\tau^*$ , is computed from (24).

On the perturbation boundary segment of  $\partial\Omega$ , we have Dirichlet boundary conditions on the perturbation velocity:  $\mathbf{u} = \mathbf{u}_c = \hat{\mathbf{u}}_c f(t, \omega)$  in which the temporal function  $f(t, \omega)$  is prescribed, and the spatial function  $\hat{\mathbf{u}}_c$  is the object to optimise. On this segment the adjoint boundary conditions are prescribed to be  $\mathbf{u}^* = 0$ , while for pressure variables we adopt consistent Neumann pressure conditions [19], which do not impose any additional restraints on the equations.

The specification of initial and boundary conditions for the LNS and adjoint equations imposes some constraints on the temporal function  $f(t, \omega)$ . We see that the initial condition for the LNS equations is set to zero, so the Dirichlet velocity condition on the perturbation boundary at  $t = 0$  has to be zero to eliminate the spatial discontinuity at the beginning of the forward integration. Further, since we require zero Dirichlet velocity conditions on the perturbed boundary for the adjoint equations, the initial condition for the adjoint equations, which is scaled from the final condition of the LNS equations by (24), has to be zero on the perturbation boundary, and therefore the final condition  $\mathbf{u}(\tau)$  has to be zero on the perturbation boundary, which requires  $\mathbf{u}_c = 0$  at  $t = \tau$ . To satisfy these compatibility requirements, the time-dependence function should satisfy  $f(0, \omega) = f(\tau, \omega) = 0$ . The form of the function chosen for the present study is presented in Section 5.2.3.

The outflow boundary segment deserves additional attention. We can use  $\mathbf{u} = 0$  for  $m \neq 0$ , as presented in [15], but at  $m = 0$ , the mass flux into the domain from the perturbation boundary may be non-zero, and so a zero-Dirichlet outflow condition violates the mass conservation law. A new outflow boundary condition is therefore adopted to avoid this violation. For the forward integration it is a typical zero-Neumann outflow condition:  $\nabla_n \mathbf{u} = 0, p = 0$ , while for the backward integration it is a Robin condition,  $\nabla_n \mathbf{u}^* + \text{Re} \mathbf{U}_n \mathbf{u}^* = 0, p^* = 0$ . Inspecting Eq. (5), one notes that the integral over the outflow boundary under these specifications is zero. At  $m \neq 0$ , the zero-Dirichlet outflow boundary condition and the new condition yield the same result within machine precision, providing that the computational domain is adequately long for the perturbation not to leave the domain. However this new outflow condition (Neumann for forward integration and Robin for backward integration) is suitable for general-sized domains and is adopted in the current study.

For the remaining boundaries, the boundary condition for the LNS equations and adjoint equations are the same. For example, on a cylindrical axis boundaries, the boundary conditions for velocity and pressure variables are zero-Dirichlet or zero-Neumann, depending on the azimuthal wave numbers, as outlined in [18] in combinations that also make no contribution to the integral term in Eq. (5); on far-field segments, zero Dirichlet velocity conditions and computed Neumann pressure conditions are adopted for the velocity components and pressure term in both LNS equations and the adjoint equations. The optimisation procedure is analogous to that used to calculate optimal initial perturbations (A).

#### 4.2. Eigenvalue approach

The boundary perturbation optimisation problem can be also transformed into an eigenvalue problem. Similar to the analysis of the optimal initial condition problem, we denote  $\mathcal{M}_c$  as an evolution operator such that

$$\mathbf{u}_\tau = \mathcal{M}_c \hat{\mathbf{u}}_c, \tag{27}$$

with dual operator  $\mathcal{M}_c^*$

$$\mathbf{g} = \mathcal{M}_c^* \mathbf{u}_\tau^*. \tag{28}$$

Comparing the Lagrangian functional before and after the integration by parts as shown in (20) and (21), we note that  $\mathcal{M}_c$  and  $\mathcal{M}_c^*$  satisfy the duality relation arising from the last two terms in Eq. (5)

$$(\mathbf{a}, \mathcal{M}_c \mathbf{b}) = [\mathcal{M}_c^* \mathbf{a}, \mathbf{b}] \quad \text{where } \mathbf{a} \in \Omega, \quad \mathbf{b} \in \partial\Omega. \tag{29}$$

Using relationships (27)–(29) in the Lagrangian functional, we obtain

$$\mathcal{L}_c = \frac{(\mathbf{u}_\tau, \mathbf{u}_\tau)}{[\hat{\mathbf{u}}_c, \hat{\mathbf{u}}_c]} = \frac{[\mathcal{M}_c^* \mathcal{M}_c \hat{\mathbf{u}}_c, \hat{\mathbf{u}}_c]}{[\hat{\mathbf{u}}_c, \hat{\mathbf{u}}_c]}.$$

Clearly the maximum value of  $\mathcal{L}_c$  and the corresponding optimal boundary perturbation are the largest eigenvalue of the operator  $\mathcal{M}_c^* \mathcal{M}_c$  and the associated eigenvector. Recalling (24) and using (27) and (28), we observe that the joint action of  $\mathcal{M}_c$  and  $\mathcal{M}_c^*$  on the boundary perturbation  $\hat{\mathbf{u}}_c$  can be expressed as

$$\mathcal{M}_c^* \mathcal{M}_c \hat{\mathbf{u}}_c = \mathcal{M}_c^* \mathbf{u}_\tau = \mathbf{g} \frac{[\hat{\mathbf{u}}_c, \hat{\mathbf{u}}_c]}{2}. \tag{30}$$

Therefore when  $\hat{\mathbf{u}}_c$  becomes the leading eigenvector of  $\mathcal{M}_c^* \mathcal{M}_c$ ,  $\mathbf{g}$  is parallel to the vector  $\hat{\mathbf{u}}_c$  and the corresponding eigenvalue is  $[\mathbf{g}, \hat{\mathbf{u}}_c]/2$ .

Similarly to the analysis presented in Section 3.2, it can be demonstrated that the Lagrangian functional  $\mathcal{L}_c$  has only one maximiser, which is the leading eigenvector of  $\mathcal{M}_c^* \mathcal{M}_c$ , where the maximum value of  $\mathcal{L}_c$  is the corresponding largest eigenvalue; and only one minimiser, provided by the eigenvector associated with the smallest eigenvalue of  $\mathcal{M}_c^* \mathcal{M}_c$ , which is the minimum value of  $\mathcal{L}_c$ . All the other eigenvectors of  $\mathcal{M}_c^* \mathcal{M}_c$  are inflection points of the Lagrangian functional [15].

Therefore an eigenvalue solver can be employed as an alternative to the optimisation method to calculate the optimal boundary perturbation. We start from an initial guess of the boundary perturbation, evolve it forwards in the LNS equations, use the final condition to initialise the adjoint LNS equation, evolve the adjoint variable backwards to obtain  $\mathbf{g}$  (which must be evaluated throughout the integration interval), and then use  $\mathbf{g}$  to initialise the LNS equations to repeat this cycle. This iterative action of the joint operator on the initial boundary perturbation builds a Krylov sequence and an Arnoldi method can be used to extract the eigenvalue/vectors of the joint operator from the sequence.

Analogously to the case for the optimal initial perturbation discussed earlier, if the matrix form of the forward operator  $\mathcal{M}_c$  is available, we can obtain the optimal boundary perturbation, optimal gain and optimal response from the singular value decomposition of  $\mathcal{M}_c$ :

$$\mathcal{M}_c \mathbf{U}_{ci} = \sigma_{ci} \mathbf{V}_{ci}. \tag{31}$$

The right and left singular vectors  $\mathbf{U}_{ci}$  and  $\mathbf{V}_{ci}$  form two orthogonal bases, and they are normalised so that  $[\mathbf{U}_{ci}, \mathbf{U}_{ci}] = 1$  and  $[\mathbf{V}_{ci}, \mathbf{V}_{ci}] = 1$ . The singular values  $\sigma_{ci}$  are real and positive. Clearly the largest singular value is the square root of the optimal gain and the corresponding right and left singular vectors are the optimal boundary perturbation and the optimal outcome. This singular value decomposition approach is a direct method and only the forward operator  $\mathcal{M}_c$  is involved. In general global studies, the matrix form of  $\mathcal{M}_c$  is not available and an iterative method such as an optimisation or eigenvalue method must be adopted to calculate the optimal boundary perturbation.

## 5. Case study for a vortex flow

### 5.1. Numerical model of the vortex flow

In this section, we implement the algorithms presented above to calculate the optimal initial and inflow boundary perturbations to the Batchelor vortex. The Batchelor vortex is a solution to the Navier–Stokes equations under a boundary-layer-type approximation obtained by [20] and it has been used extensively as a mathematical model of vortices. The Batchelor vortex can be represented in the cylindrical coordinates  $(z, r, \theta)$  as

$$U(r) = a + \exp(-r^2), \quad V(r) = 0, \quad W(r) = \frac{q}{r} [1 - \exp(-r^2)], \tag{32}$$

where  $a$  designates the free stream velocity and  $q$  is the swirl strength. Two values of the swirl strength,  $q = 0.8$  and  $q = 3$ , are considered in this study. At the first value of  $q = 0.8$ , strong helical instability are observed [21,22], while at the second value of  $q = 3$ , the vortex is asymptotically stable but exhibit reasonably strong transient energy growth [23], due to the interaction of the highly non-orthogonal eigenmodes in the continuous spectrum [24].

The Reynolds number is defined as  $Re = \Delta U R_0 / \nu$ , where  $\Delta U$  is the dimensional velocity excess in the core of the vortex,  $R_0$  is defined as the radial coordinate where the non-dimensionalised streamwise velocity  $U = 1 + \exp(-1)$  and  $\nu$  is the kinematic viscosity. The vortex core is defined as  $r = 1.12$ , where the azimuthal velocity reaches a maximum.  $Re = 100$  is used throughout this study.

Since optimal initial perturbations for the Batchelor vortex have been thoroughly investigated, we focus on optimal boundary perturbations and introduce the boundary perturbation at the inflow boundary. Firstly we validate the methodology presented above and demonstrate that the two approaches (optimisation approach and eigenvalue approach) yield the same results in subsection 5.2 and then present the results of optimal inflow boundary perturbations at  $q = 0.8$  and  $q = 3$  in subsection 5.3.

### 5.2. Discretisation and convergence

#### 5.2.1. Discretisation

The LNS equations and adjoint equations are spatially discretised following the spectral/hp element method as described by [25]. A stiffly stable velocity correction scheme [19] is applied. Details of the discretisation and its convergence properties are given by [18]. The boundary conditions implemented are as discussed in Section 4.1.

In this numerical method, we construct a weak approximation of the governing equations by multiplying a test function that vanishes on the boundary. Therefore the solution of the governing equations are required to be in the Sobolev space of order one (have square-integrable derivatives). Then it is necessary that the boundary perturbations can be extended

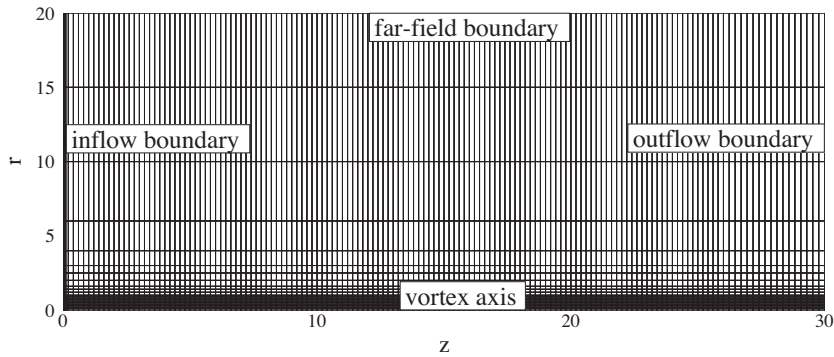


Fig. 2. Computational mesh and boundaries.

continuously into a function in the Sobolev space of order one. This restriction of the form of boundary perturbations can be relaxed to be merely square-integrable by calculating very weak solutions of the governing equations, as discussed in [26].

The computational mesh containing 3150 elements, as well as the different types of boundaries are shown in Fig. 2. Each element is further decomposed into  $P \times P$  sub-elements using a spectral element discretisation.

5.2.2. Convergence of the optimal initial perturbation

The convergence of energy growth  $G$  of initial perturbations with respect to  $P$  is shown in Table 1. We see that both the optimisation method and eigenvalue method converge to the same values of optimal energy growth with six significant figures at  $P = 5$ .

The convergence speeds of the optimal energy growth and optimal initial perturbation for both methods are reported in Fig. 3. The convergence criteria for the optimal energy growth and the optimal initial perturbation are respectively defined as  $r_{\text{ovalue}} = (G^k - G^{40})/G^{40}$  and  $r_{\text{ovector}} = 1 - (\mathbf{u}_0^k, \mathbf{u}_0^{40})/[(\mathbf{u}_0^{40}, \mathbf{u}_0^{40})(\mathbf{u}_0^k, \mathbf{u}_0^k)]^{1/2}$ , where the superscript denotes the index of iterations. We see that the eigenvalue method converges much faster than the optimisation method, owing to the large dimension of the joint operator, which has  $N - 2$  inflection points, where the gradient of the Lagrangian functional with respect to the initial perturbation vanishes, and therefore decelerates the convergence of the gradient in the optimisation solver.

5.2.3. Convergence of the optimal boundary perturbation

As stated previously, we decompose the temporal and spatial dependence of the boundary perturbation and optimise the spatial distribution of the perturbation associated with a temporal function

Table 1

Convergence of the energy growth of the optimal initial perturbation  $G$  with respect to  $P$  at  $(q, a, \tau, m) = (0.8, 0, 10, 3)$  using both the optimisation (OPT) and eigenvalue (EIG) methods. The Reynolds number is set to  $Re = 100$  hereafter.

$P$	$G$ (OPT)	$G$ (EIG)
3	18.4950	18.4950
4	18.5109	18.5109
5	18.5107	18.5107
6	18.5107	18.5107
7	18.5107	18.5107

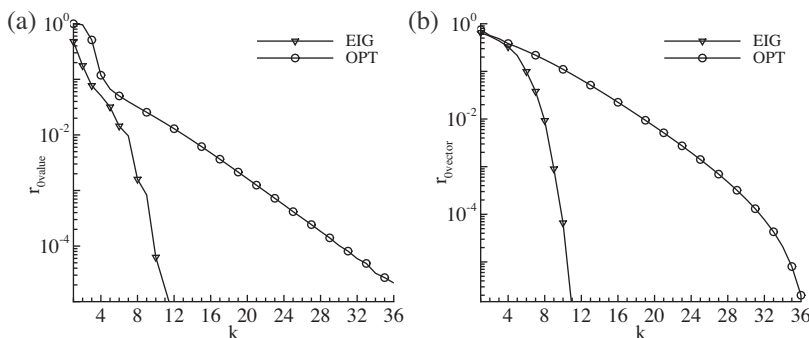


Fig. 3. Comparison of the convergence speed of (a) optimal energy growth and (b) optimal initial perturbation at  $(q, a, \tau, m) = (0.8, 0, 10, 3)$  for the optimisation method and eigenvalue method.

$$f(t, \omega) = [1 - \exp(-t^2)]\{1 - \exp[-(\tau - t)^2]\} \exp(i\omega t), \tag{33}$$

where the first two factors on the right side yield a boundary perturbation starting smoothly from zero and terminating smoothly to zero, as illustrated in Fig. 4. These two factors are used to eliminate the spatial and temporal discontinuities as discussed in Section 4.1. A similar form of temporal function was employed in [15]. We see that for large enough values of  $\tau$ , when  $0 \ll t \ll \tau, f(t, \omega) \approx \exp(i\omega t)$  and so  $\omega$  acts as the temporal frequency of the boundary perturbation. Clearly the adjoint of this function is  $f^*(t, \omega) = f(t, -\omega)$ .

As a convergence test, we consider the gain  $K$  as a function of the polynomial order for both the optimisation method and eigenvalue method, as reported in Table 2. We see that both methods converge to four significant figures at  $P = 6$ . For the optimisation method, we have tested the steepest gradient method, conjugate gradient method and BFGS quasi-Newton method to calculate the search direction and observe that the value of  $K$  is independent of the choice of these optimisation methods.

In the last column of Table 2, we also show the correctness of the gradient of the Lagrangian functional, where  $\delta \hat{\mathbf{u}}_c$  is an arbitrary vector with a small enough magnitude and  $\delta \mathcal{L}_c = \mathcal{L}_c(\hat{\mathbf{u}}_c + \delta \hat{\mathbf{u}}_c) - \mathcal{L}_c(\hat{\mathbf{u}}_c)$  is obtained by evolving the boundary perturbations in the LNS equations only. We see that the gradient  $\nabla_{\hat{\mathbf{u}}_c} \mathcal{L}_c$  obtained through evolving the perturbation in both the LNS equations and the adjoint equations is accurate within a tolerance of 0.03% at  $P = 6$ .

The convergence speeds of the optimal gain and optimal boundary perturbation for both optimisation method and eigenvalue method are reported in Fig. 5. The convergence criteria are defined as  $r_{\text{cvalue}} = (K^k - K^{10})/K^{10}$  and  $r_{\text{cvector}} = 1 - [\hat{\mathbf{u}}_c^k, \hat{\mathbf{u}}_c^{10}] / \{[\hat{\mathbf{u}}_c^{10}, \hat{\mathbf{u}}_c^{10}][\hat{\mathbf{u}}_c^k, \hat{\mathbf{u}}_c^k]\}^{1/2}$ , where the superscript denotes the index of iterations. We see that in contrast to what was observed for the calculation of optimal initial conditions, the optimisation method converges a little faster than

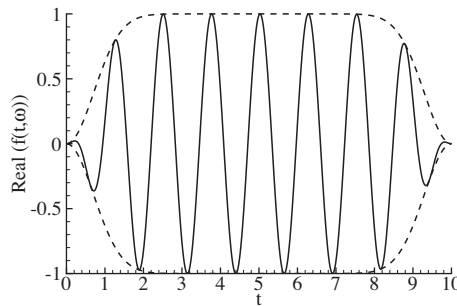


Fig. 4. Real part of the temporal dependence of the boundary velocity perturbation at  $\tau = 10$  and  $\omega = 5$ . Dashed lines represent the envelope of the function.

Table 2  
Convergence of the optimal boundary perturbations at  $(q, a, \tau, \omega, m) = (0.8, 0, 10, 0, 3)$ .

$P$	$K(\text{OPT})$	$K(\text{EIG})$	$\delta K / [\nabla_{\hat{\mathbf{u}}_c} K, \delta \hat{\mathbf{u}}_c]$
3	6.944	6.721	0.9665
4	6.982	6.951	0.9987
5	6.983	6.980	0.9993
6	6.983	6.983	0.9997
7	6.983	6.983	0.9998

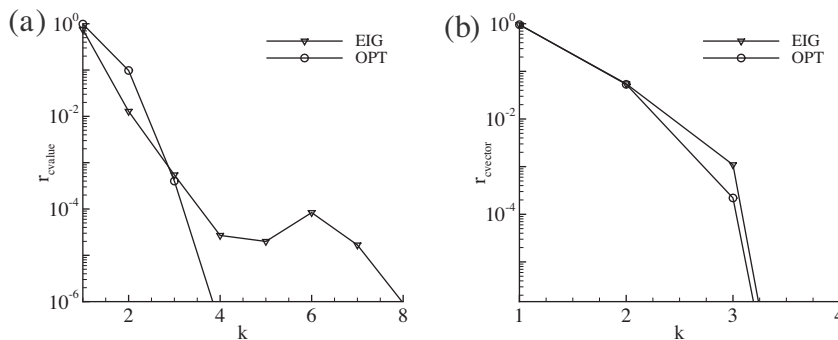


Fig. 5. Comparison of the convergence speed of (a) optimal gain and (b) optimal inflow boundary perturbation at  $(q, a, \tau, \omega, m) = (0.8, 0, 10, 0, 3)$  for the optimisation method (OPT) and eigenvalue method (EIG).

the eigenvalue method. This is because of the low dimension of the operator  $\mathcal{M}_c^* \mathcal{M}_c$ , which has many fewer inflection points than the operator  $\mathcal{M}_0^* \mathcal{M}_0$  discussed in the optimal initial condition problem.

5.3. Optimal inflow boundary perturbations for the Batchelor vortex

5.3.1. Asymptotically unstable flow with  $q = 0.8$

Four azimuthal wave numbers,  $m = 0, 1, 2, 3$ , are investigated at  $q = 0.8$ . The Batchelor vortex has helical unstable modes at  $m = 1, 2, 3$ . Since the axisymmetric mode has significant physical relevance to the bubble-type vortex breakdown, the  $m = 0$  case is also considered even though this axisymmetric mode is locally stable/weakly unstable.

As illustrated in Fig. 6(a), the gain  $K$  does not grow exponentially with  $\tau$  at  $\omega = 0$ . This is because the development of perturbations in the domain is a mixture of spatial instabilities and temporal instabilities, especially at small values of  $\tau$ , provided that the axial length of the domain is fixed. Therefore the growth rate is larger than the energy growth of the most unstable eigenmode that can be obtained by imposing periodic inflow/outflow boundary conditions. Owing to the helical instability at the combination of parameters considered here, the value of  $K$  keeps increasing with  $\tau$  and we only consider a limited range of time intervals  $0 \leq \tau \leq 15$ . The development of boundary perturbations is most energetic at  $m = 2$  for the combination of parameters considered, that is  $(a, q, \omega) = (0.5, 0.8, 0)$ , even though the most energetic temporal local mode is obtained at  $m = 3$ .

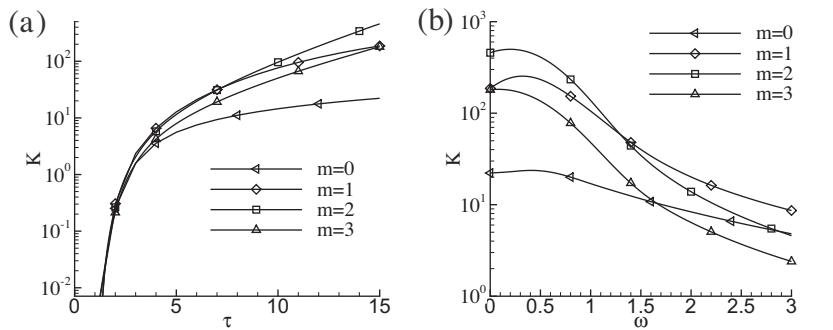


Fig. 6. Variation of the optimal gain  $K$  with (a) terminal time  $\tau$  at  $(\omega, a, q) = (0, 0.5, 0.8)$  and (b) time frequency  $\omega$  at  $(\tau, a, q) = (15, 0.5, 0.8)$ .

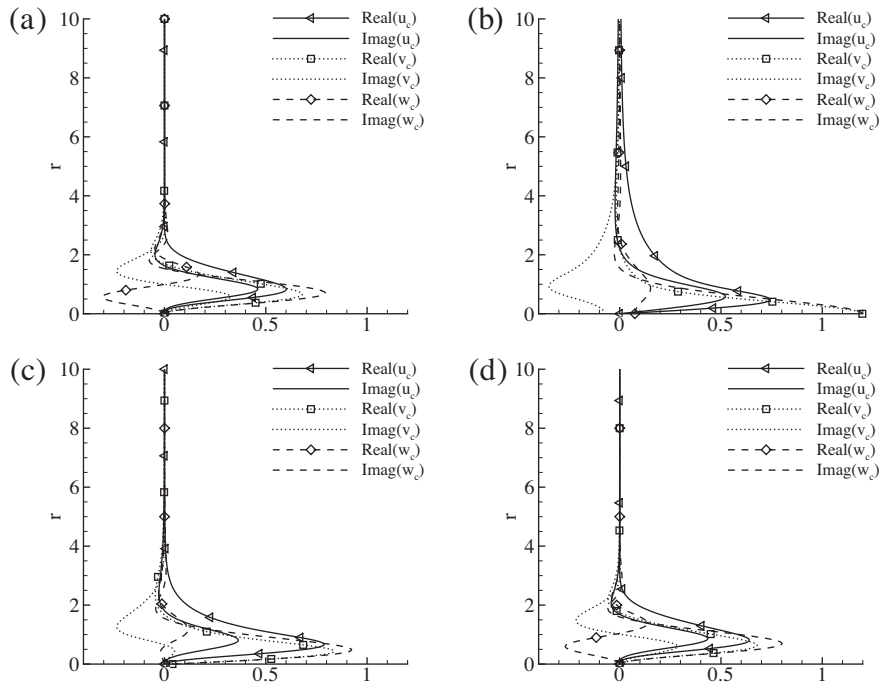
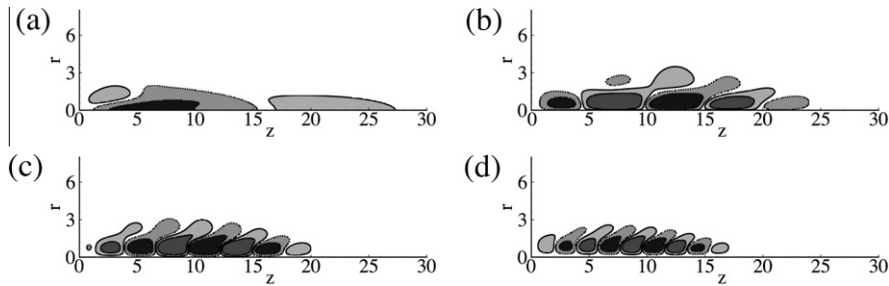


Fig. 7. Velocity components of optimal boundary perturbations at (a)  $(q, m, \omega, \tau) = (0.8, 0, 0, 15)$ , (b)  $(q, m, \omega, \tau) = (0.8, 1, 0.3, 15)$ , (c)  $(q, m, \omega, \tau) = (0.8, 2, 0.2, 15)$  and (d)  $(q, m, \omega, \tau) = (0.8, 3, 0.1, 15)$ . The boundary perturbation has been normalised such that  $[\hat{u}_c, \hat{v}_c] = 1$ .



**Fig. 8.** Contours of the axial velocity component of the outcomes of the optimal inflow boundary conditions at (a)  $(q, m, \omega, \tau) = (0.8, 0, 0.4, 15)$ , (b)  $(q, m, \omega, \tau) = (0.8, 1, 0.3, 15)$ , (c)  $(q, m, \omega, \tau) = (0.8, 2, 0.2, 15)$  and (d)  $(q, m, \omega, \tau) = (0.8, 3, 0.1, 15)$ . The boundary perturbation has been normalised so that  $[\hat{\mathbf{u}}_c, \hat{\mathbf{u}}_c] = 1$ . The same contour levels,  $[-0.5, 0.5]$ , are used on all the subfigures. Dashed/solid lines denote negative/positive velocity respectively.

Fig. 6(b) illustrates that the maximum gain at a fixed value of  $\tau = 15$  is obtained at  $\omega = 0.3, 0.2, 0.1$  for  $m = 1, 2, 3$ , respectively. These values are close to the frequencies of the most unstable helical modes. For example, the most unstable local mode obtained at  $m = 2$  has frequency 0.22.

Inspecting the optimal inflow boundary conditions shown in Fig. 7, it is seen that the energy of the optimal boundary perturbation is concentrated in the region close to the vortex axis, which is similar to the unstable helical modes [21]. In this figure, the temporal frequency  $\omega$  is chosen to maximise the gain  $K$ .

Evolving optimal inflow boundary perturbations to  $t = \tau = 15$ , we see the contours of azimuthal vorticity for these outcomes in Fig. 8. These final outcomes are the result of the spatial and temporal evolution of optimal boundary conditions and they have a similar structure to the unstable helical modes [21]. The dominant axial wave numbers of these outcomes are close to the axial wave numbers of the most unstable helical modes. We see that the structures are in the form of spirals at  $m = 1, 2, 3$  and bubbles around the axis at  $m = 0$ . Note that the boundary perturbations have been normalised so that  $[\hat{\mathbf{u}}_c, \hat{\mathbf{u}}_c] = 1$ .

5.3.2. Asymptotically stable flow with  $q = 3$

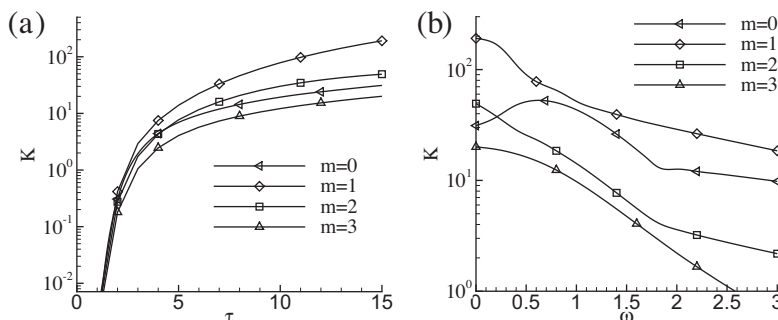
At larger swirl number,  $q = 3$ , the vortex flow is asymptotically stable but significant transient energy growth has been observed owing to the non-orthogonality of the continuous eigenmodes [27]. Two mechanisms of transient growth have been identified: the anti-lift-up mechanism associated with the transformation of azimuthal velocity into azimuthal vorticity, and the Orr-induction mechanism associated with the energy transfer from the potential region into the vortex core [28].

Fig. 9 illustrates the variation of the gain  $K$  with the time interval  $\tau$  and the temporal inflow boundary frequency  $\omega$ . It is seen that the values of  $K$  are slightly lower than those in the asymptotically unstable cases with  $q = 0.8$ . Again, the gain increases faster at small values of  $\tau$  owing to the mixing of temporal and spatial developments of perturbations.

At a fixed  $\tau$ , the maximum  $K$  is obtained at  $\omega_{\max} = 0.62$  for the axisymmetric case and at  $\omega = 0$  for all the other cases considered. This ‘frequency selection’ will be discussed in detail and compared against the optimal initial perturbations in the following.

It is noted that the optimal boundary perturbations are concentrated in the potential flow region (see Fig. 10), rather than inside the vortex core as those obtained in the asymptotically unstable conditions (see Fig. 7). Similar to the structures of the optimal initial perturbations [27], the swirl velocity component dominates in the boundary perturbations except at  $m = 1$ . Two typical cases,  $m = 0$  and  $m = 1$  are discussed below.

At  $m = 0$ , the transient growth based on both initial perturbations and boundary perturbations is mainly due to the transformation of azimuthal velocity to azimuthal vorticity while the energy distribution in the radial direction is almost unchanged (see Figs. 10(a) and 11(a) for the development of boundary perturbations and Figs. 12(a) and 12(b) for the development of initial perturbations). The dominant axial wave numbers for the outcomes of optimal initial perturbations



**Fig. 9.** (a) Variation of the gain  $K$  with terminal time  $\tau$  at  $\omega = 0$  and (b) variation of  $G$  with time frequency  $\omega$  for  $\tau = 15$  at  $a = 0.5$  and  $q = 3$ .

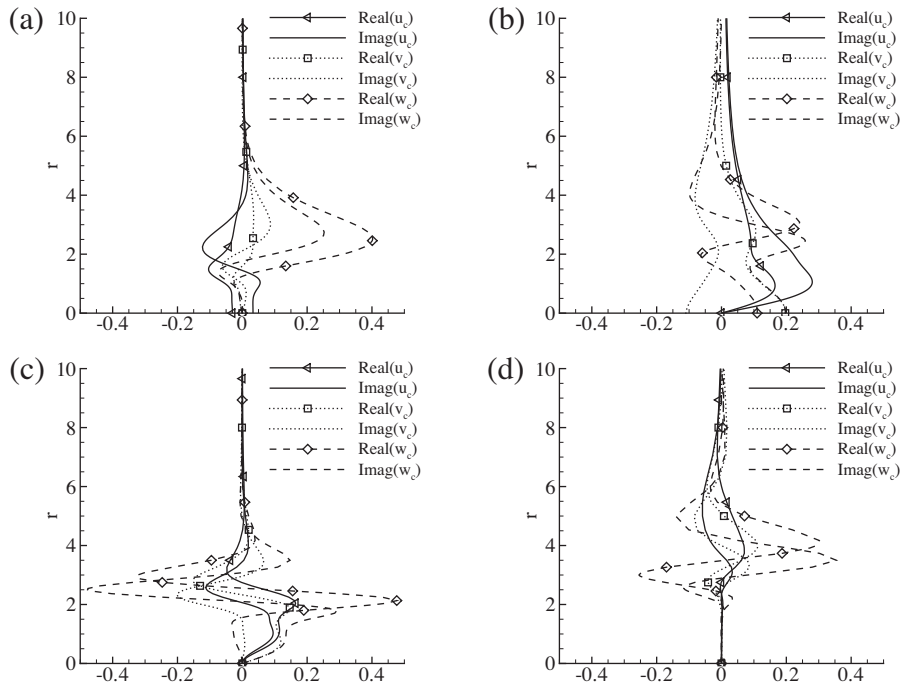


**Fig. 10.** Velocity components of optimal boundary perturbations at (a)  $(q, m, \omega, \tau) = (3, 0, 0.6, 15)$ , (b)  $(q, m, \omega, \tau) = (3, 1, 0, 15)$ , (c)  $(q, m, \omega, \tau) = (3, 2, 0, 15)$  and (d)  $(q, m, \omega, \tau) = (3, 3, 0, 15)$ . The boundary perturbation has been normalised so that  $[\bar{\mathbf{u}}_c, \bar{\mathbf{u}}_c] = 1$ .

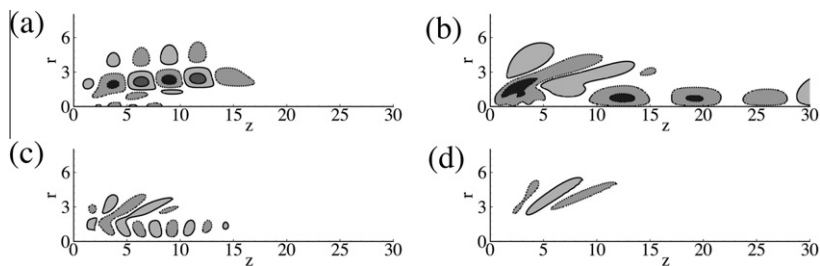


**Fig. 11.** Contours of the axial velocity component of the outcomes of the optimal inflow boundary conditions at (a)  $(q, m, \omega, \tau) = (3, 0, 0.6, 15)$ , (b)  $(q, m, \omega, \tau) = (3, 1, 0, 15)$ , (c)  $(q, m, \omega, \tau) = (3, 2, 0, 15)$  and (d)  $(q, m, \omega, \tau) = (3, 3, 0, 15)$ . The boundary perturbation has been normalised so that  $[\bar{\mathbf{u}}_c, \bar{\mathbf{u}}_c] = 1$ . The same contour levels,  $[-0.5, 0.5]$ , are used on all the subfigures. Dashed/solid lines denote negative/positive velocity respectively.

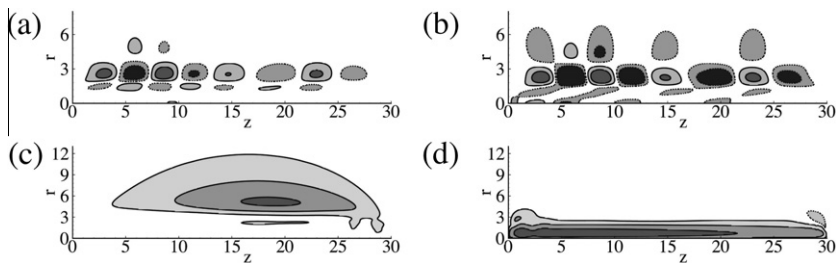


**Fig. 12.** Contours of the axial velocity component of (a), optimal initial perturbation at  $m = 0$ , (b), optimal final perturbation at  $m = 0$ , (c), optimal initial perturbation at  $m = 1$  and (d), optimal final perturbation at  $m = 1$ . The contour levels are selected to highlight the structures of perturbations.

and optimal boundary perturbations are the same, that is  $k_{\max} = 1.14$ . The optimal temporal frequency of the boundary perturbations reflects this axial wave number selection:  $2\pi a/\omega_{\max} \approx 2\pi/k_{\max}$ .

At  $m = 1$ , the transient growth from both initial perturbations and boundary perturbations results from the energy transfer from the potential region into the vortex core. From the outcomes of the optimal boundary perturbation shown in Fig. 11,

it is observed that the energy has been introduced from the potential region into the vortex core at  $m = 1$ . This link between the potential region and vortex core can be explained by the non-normality of eigenmodes with the form of two wave packets – one inside the vortex core and the other in the potential region [27]. This energy transfer also appears at  $m = 0$ , where a string of bubble-type structures are induced along the axis but the distribution of major structures are static, as shown in Fig. 12(b).

### 6. Conclusion

Constraint Lagrangian functionals are built in order to calculate optimal initial and boundary perturbations which induce maximum energy in the domain at a fixed time horizon. In our analysis we have demonstrated that both Lagrangian optimisation problems can be transformed into eigenvalue methods. The optimal energy growth/gain and optimal initial/boundary perturbations are the leading eigenvalue/eigenvector of a joint operator, whose action is related to the LNS equations and the adjoint equations. When optimising the inflow boundary perturbations, a temporally smooth function which is zero at both the beginning and end of the integration is adopted so as to eliminate spatial and temporal discontinuities. A new out-flow boundary condition is adopted to avoid the possible violation of mass conservation in the mean Fourier mode ( $m = 0$ ).

We applied these methods to a vortex flow, modelled by the Batchelor vortex, to calculate optimal initial/inflow boundary perturbations. Via a convergence test, it is shown that both optimisation and eigenvalue methods converge to the same results. In the optimal initial condition problem, the eigenvalue approach converges much faster than the optimisation approach, because the large dimension of the joint operator generates a large number of inflection points and decelerates the convergence of the gradient optimisation method. On the other hand, in the boundary condition problem, where the dimension of the joint operator is much smaller than that in the initial condition problem, both methods show fast convergence for the test problem.

For the asymptotically unstable conditions, the optimal perturbation for the vortex flow takes a similar form to the most unstable local mode – both have the energy concentrated inside the vortex core. The maximum gain  $K$  is obtained at the temporal frequency of the most unstable local mode and the dominant axial wave number of the final outcome is the same as the wave number of the most unstable helical mode. For the asymptotically stable conditions, the optimal perturbations are similar to the optimal initial perturbations. When  $m = 0$ , the anti-lift-up mechanism associated with energy transfer from azimuthal velocity to azimuthal vorticity is observed in both the boundary condition and initial condition transient processes. When  $m > 0$ , the Orr-induction mechanism associated with core contamination is also observed in the development of both the optimal initial and boundary perturbations.

### Acknowledgements

We would like to acknowledge financial support from the Australian Research Council through Discovery Program Grant DP1094851, and from Australia’s National Computational Infrastructure via Merit Allocation Scheme Grant D77. SJS would like to acknowledge financial support under EPSRC grant EP/H050507/1.

### Appendix A. Optimisation procedure

The optimisation procedure to maximise the Lagrangian functional and obtain the optimal initial condition, similar to the algorithm outlined by [2], is as follows:

1. Evolve an initial guess of the optimal initial perturbation  $\mathbf{u}_0$  to obtain  $\mathbf{u}_\tau$  by integrating the LNS Eq. (1) forwards from  $t = 0$  to  $t = \tau$ .
2. Scale  $\mathbf{u}_\tau$  using (9) to obtain the initial condition of the adjoint equations  $\mathbf{u}_\tau^*$ .
3. Evolve  $\mathbf{u}_\tau^*$  using (4) to obtain  $\mathbf{u}_0^*$  by integrating the adjoint velocity backwards from  $t = \tau$  to  $t = 0$ .
4. Substitute  $\mathbf{u}_\tau$ ,  $\mathbf{u}_0$  and  $\mathbf{u}_0^*$  into (11) to obtain  $\nabla_{\mathbf{u}_0} \mathcal{L}_0$ .
5. Update the initial perturbation from step  $k$  to  $k + 1$ , such that  $\mathbf{u}_0^{k+1} = \mathbf{u}_0^k + \alpha^k \mathcal{P}(\nabla_{\mathbf{u}_0} \mathcal{L}_0)^k$ , where  $\alpha$  is a step length and  $\mathcal{P}(\nabla_{\mathbf{u}_0} \mathcal{L}_0)^k$  is a search direction.
6. Repeat (2)–(6) until the energy growth  $G$  converges.

Three methods (steepest gradient, conjugate gradient, BFGS) are considered to calculate the search direction [29]. In the steepest gradient method,

$$\mathcal{P}(\nabla_{\mathbf{u}_0} \mathcal{L}_0)^k = (\nabla_{\mathbf{u}_0} \mathcal{L}_0)^k;$$

in the (Fletcher–Reeves) conjugate gradient method,

$$\begin{aligned} \mathcal{P}(\nabla_{\mathbf{u}_0} \mathcal{L}_0)^0 &= (\nabla_{\mathbf{u}_0} \mathcal{L}_0)^0, \\ \mathcal{P}(\nabla_{\mathbf{u}_0} \mathcal{L}_0)^k &= (\nabla_{\mathbf{u}_0} \mathcal{L}_0)^k + \frac{((\nabla_{\mathbf{u}_0} \mathcal{L}_0)^k, (\nabla_{\mathbf{u}_0} \mathcal{L}_0)^k)}{((\nabla_{\mathbf{u}_0} \mathcal{L}_0)^{k-1}, (\nabla_{\mathbf{u}_0} \mathcal{L}_0)^{k-1})} \mathcal{P}(\nabla_{\mathbf{u}_0} \mathcal{L}_0)^{k-1} \quad \text{for } k > 0; \end{aligned}$$

in the BFGS method,

$$\begin{aligned} \mathcal{P}(\nabla_{\mathbf{u}_0} \mathcal{L}_0)^0 &= (\nabla_{\mathbf{u}_0} \mathcal{L}_0)^0, \\ \mathcal{P}(\nabla_{\mathbf{u}_0} \mathcal{L}_0)^k &= H^k(\nabla_{\mathbf{u}_0} \mathcal{L}_0)^k \quad \text{for } k > 0, \end{aligned}$$

where  $H^k$  is the inverse Hessian approximation

$$\begin{aligned} H^1 &= -\frac{\mathbf{y}^1 \mathbf{s}^1}{\mathbf{y}^1 \mathbf{T} \mathbf{y}^1} I, \\ H^{k+1} &= (I - \rho^k \mathbf{s}^k \mathbf{y}^k \mathbf{T}) H^k (I - \rho^k \mathbf{y}^k \mathbf{s}^k \mathbf{T}) - \rho^k \mathbf{s}^k \mathbf{s}^k \mathbf{T} \quad \text{for } k > 1, \end{aligned}$$

and where

$$\rho^k = \frac{1}{\mathbf{y}^k \mathbf{T} \mathbf{s}^k}, \quad \mathbf{s}^k = \mathbf{u}_0^{k+1} - \mathbf{u}_0^k, \quad \text{and} \quad \mathbf{y}^k = (\nabla_{\mathbf{u}_0} \mathcal{L}_0)^{k+1} - (\nabla_{\mathbf{u}_0} \mathcal{L}_0)^k.$$

The step length  $\alpha$  is the optimal step length that maximises

$$G^{k+1}(\alpha) = \frac{(\mathcal{M}_0(\mathbf{u}_0^k + \alpha \mathcal{P}^k), \mathcal{M}_0(\mathbf{u}_0^k + \alpha \mathcal{P}^k))}{(\mathbf{u}_0^k + \alpha \mathcal{P}^k, \mathbf{u}_0^k + \alpha \mathcal{P}^k)}.$$

Considering that  $\mathcal{M}_0$  is a linear operator, through standard algebraic manipulation we obtain

$$G^{k+1}(\alpha) = \frac{(\mathcal{M}_0 \mathcal{P}^k, \mathcal{M}_0 \mathcal{P}^k)}{(\mathcal{P}^k, \mathcal{P}^k)} + \frac{a_3 \alpha + a_4}{\alpha^2 + a_1 \alpha + a_2}, \tag{A.1}$$

where

$$\begin{aligned} a_1 &= \frac{2(\mathbf{u}_0^k, \mathcal{P}^k)}{(\mathcal{P}^k, \mathcal{P}^k)}, \quad a_2 = \frac{(\mathbf{u}_0^k, \mathbf{u}_0^k)}{(\mathcal{P}^k, \mathcal{P}^k)}, \\ a_3 &= \frac{2(\mathcal{M}_0 \mathbf{u}_0^k, \mathcal{M}_0 \mathcal{P}^k)}{(\mathcal{P}^k, \mathcal{P}^k)} - \frac{2(\mathcal{M}_0 \mathcal{P}^k, \mathcal{M}_0 \mathcal{P}^k)(\mathbf{u}_0^k, \mathcal{P}^k)}{(\mathcal{P}^k, \mathcal{P}^k)^2}, \\ a_4 &= \frac{(\mathcal{M}_0 \mathbf{u}_0^k, \mathcal{M}_0 \mathbf{u}_0^k)}{(\mathcal{P}^k, \mathcal{P}^k)} - \frac{(\mathcal{M}_0 \mathcal{P}^k, \mathcal{M}_0 \mathcal{P}^k)(\mathbf{u}_0^k, \mathbf{u}_0^k)}{(\mathcal{P}^k, \mathcal{P}^k)^2}. \end{aligned}$$

Differentiating (A.1) we see that  $G^{k+1}(\alpha)$  reaches maxima at one of the four values of  $\alpha$ :

$$\begin{aligned} \alpha_1 &= -\frac{a_4}{a_3} + \left( \frac{a_4^2}{a_3^2} + a_2 - \frac{a_1 a_4}{a_3} \right)^{1/2}, \\ \alpha_2 &= -\frac{a_4}{a_3} - \left( \frac{a_4^2}{a_3^2} + a_2 - \frac{a_1 a_4}{a_3} \right)^{1/2}, \\ \alpha_3 &= 0, \quad \alpha_4 = \infty. \end{aligned}$$

We also note that if  $a_3 \rightarrow 0$ , there is singularity when calculating  $\alpha_1$  and  $\alpha_2$ . In this condition, the values of  $\alpha_1$  and  $\alpha_2$  should be changed to

$$\alpha_1 = \alpha_2 = -\frac{a_1}{2}.$$

Substituting  $\alpha_1$ – $\alpha_4$  into (A.1) and comparing the corresponding  $G^{k+1}(\alpha)$ , we obtain the optimal value of  $\alpha$ , denoted as  $\alpha_{\max}$ . If  $\alpha_1$  or  $\alpha_2$  is complex or real but negative, this value should be removed from the comparison. If  $\alpha_3$  is the optimal value, it suggests that  $\mathbf{u}_0^k$  has converged to the optimal inflow perturbation and the optimisation should be ceased. If  $\alpha_4$  is the optimal value, it means that  $\mathbf{u}_0^k$  should be updated to be  $\mathcal{P}^k$ .

We note that  $\mathcal{P}^k$  should be evolved through the LNS equations to obtain  $a_1$ – $a_4$  and the updated outcome velocity vector  $\mathbf{u}_\tau$  can be obtained from a linear combination

$$\mathbf{u}_\tau^{k+1} = \mathcal{M}_0(\mathbf{u}_0^k) + \alpha_{\max} \mathcal{M}_0(\mathcal{P}^k). \tag{A.2}$$

Therefore step (1) for  $k > 1$  in the optimisation procedure should be replaced with

1. Evolve  $\mathcal{P}^k$  by integrating the LNS equations from  $t = 0$  to  $t = \tau$  and substitute the result velocity vector  $\mathcal{M}_0(\mathcal{P}^k)$  into (A.2) to obtain  $\mathbf{u}_\tau^{k+1}$ .

## References

- [1] L.N. Trefethen, A.E. Trefethen, S.C. Reddy, T.A. Driscoll, Hydrodynamic stability without eigenvalues, *Science* 261 (1993) 578–584.
- [2] P.J. Schmid, Nonmodal stability theory, *Annu. Rev. Fluid Mech.* 39 (2007) 129–162.
- [3] P.J. Schmid, D.S. Henningson, *Stability and Transition in Shear Flows*, Springer, 2001.
- [4] D. Barkley, H.M. Blackburn, S.J. Sherwin, Direct optimal growth analysis for timesteppers, *Int. J. Num. Methods Fluids* 57 (2008) 1437–1458.
- [5] D. Sipp, O. Marquet, P. Meliga, A. Barbagallo, Dynamics and control of global instabilities in open flows: a linearized approach, *Appl. Mech. Rev.* 63 (2010).
- [6] H.M. Blackburn, D. Barkley, S.J. Sherwin, Convective instability and transient growth in flow over a backward-facing step, *J. Fluid Mech.* 603 (2008) 271–304.
- [7] H.M. Blackburn, S.J. Sherwin, D. Barkley, Convective instability and transient growth in steady and pulsatile stenotic flows, *J. Fluid Mech.* 607 (2008) 267–277.
- [8] X. Mao, S.J. Sherwin, H.M. Blackburn, Transient growth and bypass transition in stenotic flow with a physiological waveform, *Theor. Comput. Fluid Dyn.* 25 (2011) 31–42.
- [9] P. Andersson, M. Berggren, D.S. Henningson, Optimal disturbances and bypass transition in boundary layers, *Phys. Fluids* 11 (1999) 134–150.
- [10] A. Guégan, P. Schmid, P. Huerre, Optimal energy growth and optimal control in swept Hiemenz flow, *J. Fluid Mech.* 566 (2006) 11–45.
- [11] P. Corbett, A. Bottaro, Optimal control of nonmodal disturbance in boundary layers, *Theor. Comput. Fluid Dyn.* 15 (2001) 65–81.
- [12] C.C.T. Pringle, R.R. Kerswell, Using nonlinear transient growth to construct the minimal seed for shear flow turbulence, *Phys. Rev. Lett.* 105 (2010) 154502.
- [13] A. Monokrousos, A. Bottaro, L. Brandt, A.D. Vita, D.S. Henningson, Nonequilibrium thermodynamics and the optimal path to turbulence in shear flows, *Phys. Rev. Lett.* 106 134502 (2011).
- [14] A. Monokrousos, E. Åkervik, L. Brandt, D.S. Henningson, Global three-dimensional optimal disturbances in the Blasius boundary-layer flow using time-steppers, *J. Fluid Mech.* 650 (2010) 181–214.
- [15] X. Mao, H.M. Blackburn, S.J. Sherwin, Optimal inflow boundary condition perturbations in steady stenotic flows, *J. Fluid Mech.* 705 (2012) 306–321.
- [16] D. Hill, Adjoint systems and their role in the receptivity problem for boundary layers, *J. Fluid Mech.* 292 (1995) 183–204.
- [17] M. Hogberg, D. Henningson, Linear optimal control applied to instabilities in spatially developing boundary layers, *J. Fluid Mech.* 470 (2002) 151–179.
- [18] H.M. Blackburn, S.J. Sherwin, Formulation of a Galerkin spectral element – Fourier method for three-dimensional incompressible flows in cylindrical geometries, *J. Comput. Phys.* 197 (2004) 759–778.
- [19] G.E. Karniadakis, M. Israeli, S.A. Orszag, High-order splitting methods for the incompressible Navier–Stokes equations, *J. Comput. Phys.* 97 (1991) 414–443.
- [20] G.K. Batchelor, Axial flow in trailing line vortices, *J. Fluid Mech.* 20 (1964) 645–658.
- [21] M. Lessen, P.J. Singh, F. Paillet, The stability of a trailing line vortex. Part 1. Inviscid theory, *J. Fluid Mech.* 63 (1974) 753–763.
- [22] M. Lessen, F. Paillet, The stability of a trailing line vortex. Part 2. Viscous theory, *J. Fluid Mech.* 65 (1974) 769–779.
- [23] C.J. Heaton, N. Peake, Transient growth in vortices with axial flow, *J. Fluid Mech.* 587 (2007) 271–301.
- [24] X. Mao, S.J. Sherwin, Continuous spectra of the Batchelor vortex, *J. Fluid Mech.* 681 (2011) 1–23.
- [25] G.E. Karniadakis, S.J. Sherwin, *Spectral/hp Element Methods for Computational Fluid Dynamics*, 2nd ed., Oxford University Press, 2005.
- [26] M. Berggren, Approximation of very weak solutions to boundary-value problems, *SIAM J. Numer. Anal.* 42 (2004) 860–877.
- [27] X. Mao, *Vortex instability and transient growth*, Ph.D. thesis, Imperial College London, 2010.
- [28] J. Fontane, P. Brancher, D. Fabre, Stochastic forcing of the Lamb–Oseen vortex, *J. Fluid Mech.* 613 (2008) 233–254.
- [29] J. Nocedal, S. Wright, *Numerical Optimization*, Springer, 1999.